ACS MATERIALS Au
AN OPEN ACCESS JOURNAL OF THE AMERICAN CHEMICAL SOCIETY

pubs.acs.org/materialsau Article

Enzymatic Synthesis of Xylan Microparticles with Tunable Morphologies

Peter J. Smith, Thomas M. Curry, Jeong-Yeh Yang, William J. Barnes, Samantha J. Ziegler, Ashutosh Mittal, Kelley W. Moremen, William S. York, Yannick J. Bomble, Maria J. Peña, and Breeanna R. Urbanowicz*

Cite This: *ACS Mater. Au* 2022, 2, 440–452 Read Online

ACCESS | Metrics & More | Article Recommendations | Supporting Information

ABSTRACT: Xylans are a diverse family of hemicellulosic polysaccharides found in abundance within the cell walls of nearly all flowering plants. Unfortunately, naturally occurring xylans are highly heterogeneous, limiting studies of their synthesis and structure–function relationships. Here, we demonstrate that xylan synthase 1 from the charophyte alga *Klebsormidium flaccidum* is a powerful biocatalytic tool for the bottom-up synthesis of pure β-1,4 xylan polymers that self-assemble into microparticles in vitro. Using uridine diphosphate-xylose (UDP-xylose) and defined saccharide primers as substrates, we demonstrate that the shape, composition, and properties of the self-assembling xylan microparticles could be readily controlled via the fine structure of the xylan oligosaccharide primer used to initiate polymer elongation. Furthermore, we highlight two approaches for bottom-up and surface functionalization of xylan microparticles with chemical probes and explore the susceptibility of xylan microparticles to enzymatic hydrolysis. Together, these results provide a useful platform for structural and functional studies of xylans to investigate cell wall biosynthesis and polymer–polymer interactions and suggest possible routes to new biobased materials with favorable properties for biomedical and renewable applications.

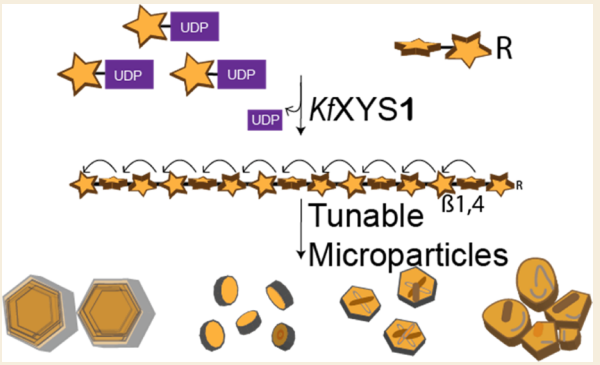

KEYWORDS: *xylan, hemicellulose, biomaterials, polysaccharide biosynthesis, xylan synthase, plant cell wall*

Xylans are polysaccharides that can account for up to 50% of the dry weight of plant cell walls and are among the most abundant biological molecules on earth. They are crucially important for many aspects of human life as they influence the nutritional aspects of the food we eat, the properties of structural materials we use, and the clothing we wear, as well as our ability to produce fuels and products from biomass.[1] For these reasons, it is of critical importance to understand the mechanisms by which xylan polymers are synthesized, as well as the dynamics of polymer–polymer interactions that govern xylan behavior in living and synthetic systems.[2] Though heterogeneous in structure, xylans from terrestrial plants have a backbone consisting of β-1,4-linked xylosyl residues and are usually heavily substituted with various substituents such as acetyl groups (linked via *O*-2, *O*-3, and *O*-2/*O*-3) and saccharides, including 4-*O*-methyl-glucuronosyl (linked via *O*-2) and arabinosyl residues (linked via *O*-2 and/or *O*-3).[1] Xylans play a major role in plant cell wall biology by interacting directly with cellulose microfibrils that make up the bulk of all plant biomass and have also been shown to interact with the polyphenolic compound lignin present within the secondary cell walls of several monocot and dicot species.[3] Current understanding in the field holds that some xylan polymers adopt a twofold screw conformation upon binding to crystalline cellulose; however, others adopt a threefold helical screw conformation depending on the distribution of their side-chain moieties or when interacting with amorphous cellulose and/or lignin (Figure 3d).[4]

The abundance of renewable sources of xylan in nature has attracted considerable attention for the utilization of this polymer as a feedstock for biobased products, and as a result, xylans have begun to be utilized to produce biomaterials such as plastics, coatings, adhesives, and packaging materials.[5] Xylans are also major dietary polysaccharides that upon ingestion are degraded and metabolized by gut microflora, making xylans essential to the development and maintenance of enteric microbial communities.[6] Therefore, xylans are considered largely biocompatible with human and animal consumption

Received: January 14, 2022
Revised: March 10, 2022
Accepted: March 14, 2022
Published: April 5, 2022

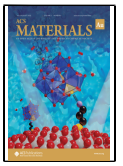

https://doi.org/10.1021/acsmaterialsau.2c00006
ACS Mater. Au 2022, 2, 440–452

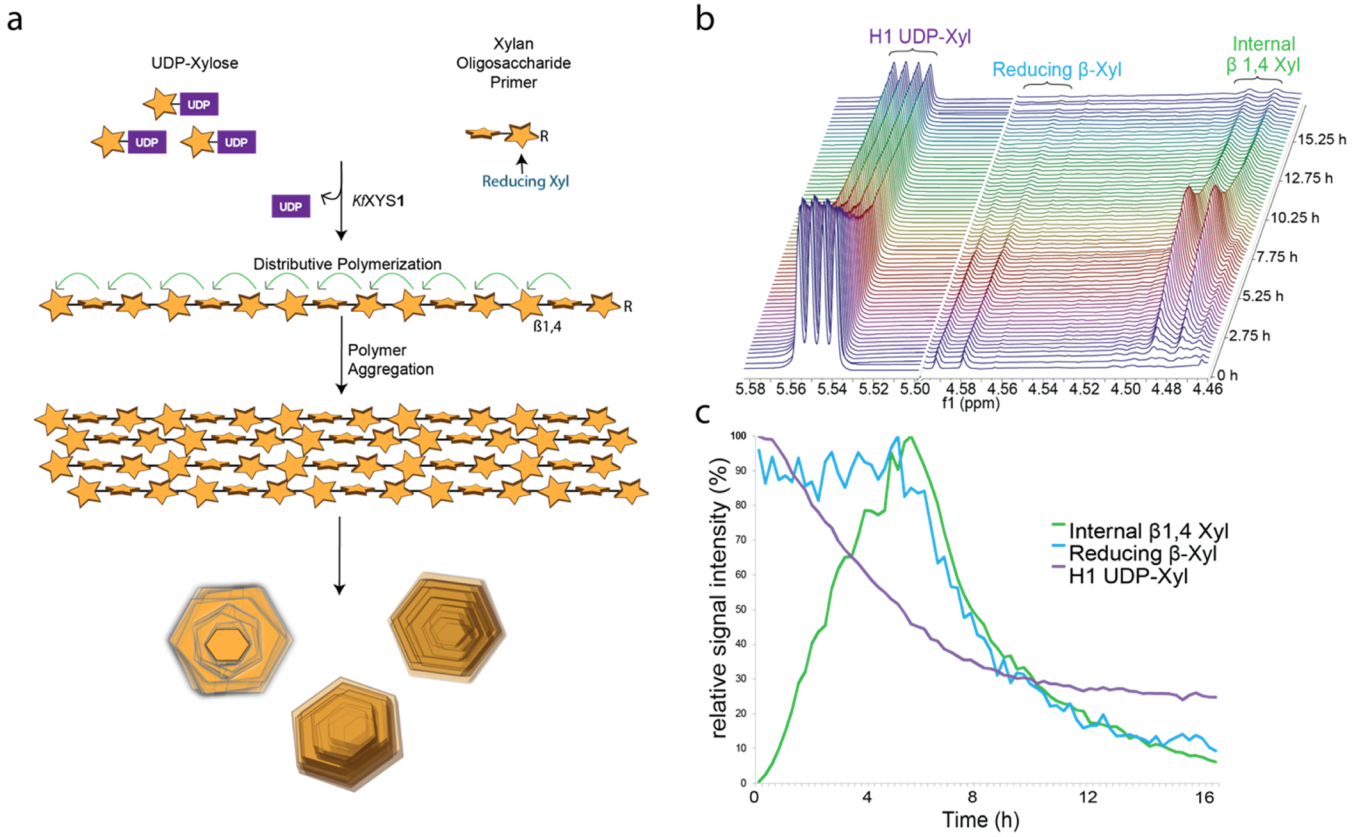

Figure 1. Enzymatic synthesis of xylan microparticles using a recombinant xylan synthase. (a) Schematic of the KfXYS1-mediated xylan synthesis and microparticle formation. Xylose from UDP-Xyl is added to XOS primers by KfXYS1 forming β-1,4-linked xylan chains that associate into microstructures. (b) Real-time ^{1}H NMR analysis of the *Kf*XYS1 xylan polymerization and precipitation. (c) Intensity (relative to maximum) of diagnostic signals of substrates and products during real-time ^{1}H NMR analysis.

and are of increasing interest for their potential as prebiotics and drug delivery vehicles due to their favorable characteristics and biocompatibility.[7]

In plants, xylans are structurally diverse and tightly associated with other components in the complex polymeric matrix that is the plant cell wall. Extraction of xylans from natural sources typically involves complicated processes and the utilization of harsh reagents. During these extraction processes, many structural features of the xylans can be modified or lost. An approach that can overcome these limitations is the production of well-defined xylan polymers by enzymatic synthesis.[8] In most organisms, complex glycans such as polysaccharides are formed through the concerted action of Leloir glycosyltransferases (GTs), which catalyze the transfer of a sugar monomer from an activated nucleotide sugar donor (NDP-sugar) to an acceptor molecule, forming glycosidic bonds in a specific manner.[9,10] Recent work has begun to uncover the mechanisms underlying xylan synthesis enzymes classified within the carbohydrate-active enzyme database (CAZY). Members of glycosyltransferase family 47 (GT47) were shown to act as xylan synthases (XYS), catalyzing the transfer of xylosyl residues from uridine diphosphate-xylose (UDP-Xyl) to xylo-oligosaccharide acceptors (XOS), forming extended xylan chains in vitro (Figure 1a).[11] The ability of GT47 family members to elongate xylan chains is a conserved function with functional orthologs of the *Arabidopsis* XYS(IRX10) present in plants as basal as the Charophyceae.[12] Furthermore, it has been shown that xylan synthases from both the model plant *Arabidopsis* and the charophycean green algae *Klebsormidium flaccidum* act in a distributive mechanism in vitro.[11,12]

GTs that catalyze glycosyl chain elongation by a distributive mechanism release the acceptor substrate after the addition of a single residue, leading to the production of products with degrees of polymerization (DP) that adhere to a Poisson distribution as the reaction progresses. Biochemical data showing that xylan is synthesized via a distributive mechanism in vitro was initially surprising as it was believed that all hemicellulose backbone synthases were members of family GT2, which function as processive glycosyltransferases, forming products with high degrees of polymerization before chain termination. This mechanism is used by synthases that generate products with high degrees of polymerization observed, where they extend single chains until the chain is terminated.[11]

Interestingly, previous studies investigating in vitro xylan synthesis have reported the formation of unsubstituted xylan oligosaccharides of lengths that exceed what is believed to be soluble in an aqueous solution.[13,14] It is expected that at high enough concentrations in solution, these polymers are able to coalesce and form insoluble and often crystalline products.[11,12,14] Several studies dating back to the mid-20th century reported the self-assembly of xylan microcrystals from hydrothermally treated xylans extracted from birch and esparto grasses.[15−19] This hydrothermal treatment appeared to remove substituents. The authors investigated the structural aspects of these crystals and determined that the polymers within exhibited a conformation consistent with a threefold screw axis of symmetry.[15−19] Interestingly, a recent report has demonstrated

https://doi.org/10.1021/acsmaterialsau.2c00006
ACS Mater. Au 2022, 2, 440−452

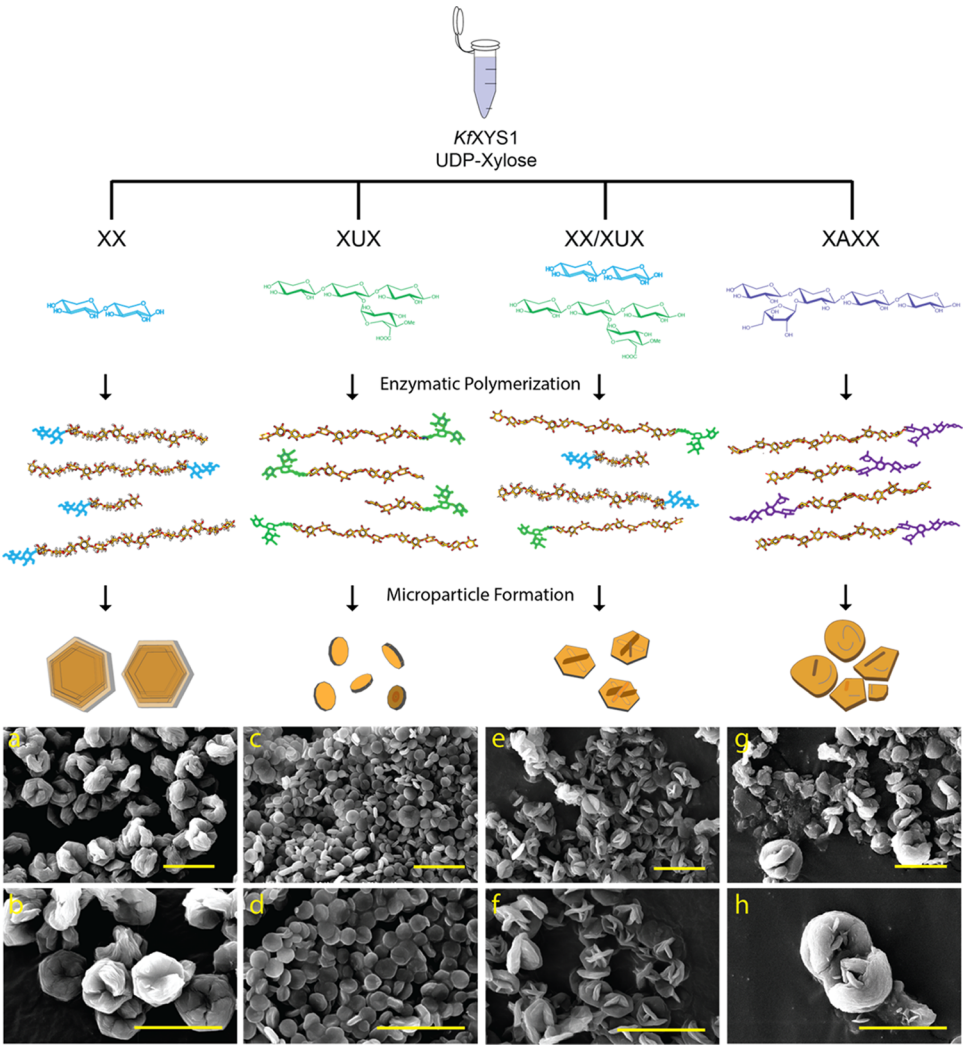

Figure 2. Morphologies of xylan microparticles formed from different xylan oligosaccharide primers. Representative scanning electron microscopy (SEM) images of (a, b) XX-type microparticles, (c, d) XUX-type particles, (e, f) XX/XUX-type particles, and (g, h) XAXX-type particles. All scale bars represent 10 μm.

the production of xylan nanocrystals via the precipitation of alkali-extracted xylan polymers in dimethyl sulfoxide (DMSO), and polymers in these nanocrystals were found to exhibit a twofold axis of symmetry.[20] Enzymatic removal of xylan side chains has been shown to influence the crystallinity of xylan aggregates, suggesting a negative correlation between the degree of substitution and crystallinity.[14,21] In addition, recent work using glycosynthases, glycoside hydrolases modified to function as transferases, demonstrated that long xylan chains can be generated by stitching together chemically synthesized xylan oligosaccharide fluorides of defined structures by repetitive condensation.[3,13] Glycosynthase-formed xylans can assemble into crystalline aggregates where the degree of crystallinity was found to be dependent not just on side-chain abundance but also on the linkage and structural features of side-chain groups decorating the polymers.[14] Further, studies have investigated the formation of xylan hydrate nanocrystals from the mild ultrasonic treatment of aqueous xylan suspensions.[22] However, the mechanisms that might govern the processes of xylan aggregation have remained largely unexplored.

In this work, we demonstrate the enzymatic synthesis of pure β-1,4 xylan polymers using a recombinant algal xylan synthase (*Kf*XYS1) and the self-assembly of the products into microparticles with tunable morphologies that are dependent on fine structural elements of the XOS primer used to initiate elongation. Furthermore, we investigate enzymatic hydrolysis and chemical routes to modify these xylan assemblies to alter their structure and properties, respectively. Taken together, we present a new enabling platform for glycosyltransferase-catalyzed xylan synthesis that can be used as a valuable tool to study both in vitro polymerization and the relationship between polymer structure and packing into high-order molecular assemblies.

RESULTS AND DISCUSSION

Optimized Xylan Synthesis by *Kf*XYS1

Previous work established that *Kf*XYS1 is a xylan synthase that catalyzes the formation of xylan via the enzymatic transfer of a xylosyl residue (Xyl) from the nucleotide sugar donor uridine diphosphate-xylose (UDP-Xyl) to XOS acceptors, such as xylobiose (XX), to form xylan oligosaccharides and polymers (Figure 1a).[12] Glycosyltransferases carry out bisubstrate reactions and are often feedback-inhibited by the accumulating UDP. In the case of this enzyme, additional experiments using a His-tagged GFP-*Kf*XYS1 fusion protein showed that little to no

https://doi.org/10.1021/acsmaterialsau.2c00006
ACS Mater. Au 2022, 2, 440−452

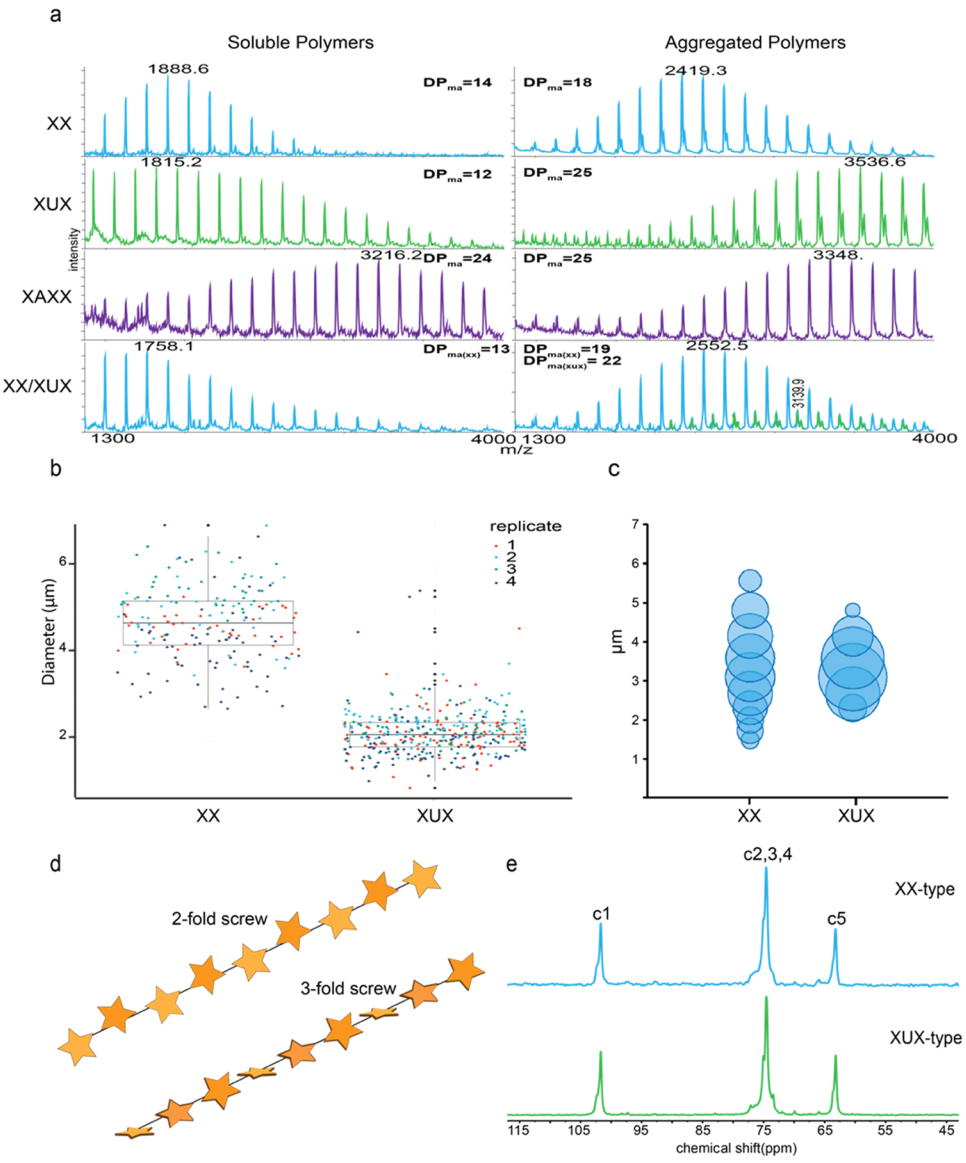

Figure 3. Characteristics of enzymatically synthesized xylans: (a) representative MALDI-TOF MS of soluble xylan polymers remaining in the supernatant after the reaction and those released from microparticles after solubilization by boiling (right). (b) Diameter of XX- and XUX-type microparticles across four replicates as measured by SEM. The mean diameter of microparticles differs significantly between primer types (two-tailed *t*-test, $P < 0.00001$ XX-type $n = 244$, XUX-type $n = 379$). (c) Dynamic light scattering (DLS) analysis of XX- and XUX-type particles. (d) Diagram of twofold vs threefold screw conformations of xylan. (e) Cross-polarized magic-angle spinning (CP-MAS) solid-state NMR analysis of XX- and XUX-type xylan microparticles. These spectra are consistent with the previously characterized xylan in a threefold screw conformation.

product inhibition occurred during in vitro xylan synthesis reactions. Furthermore, we found that xylosyl transfer continues until colloidal precipitants are formed when carried out with high ratios of donor substrate (UDP-Xyl) to acceptor substrate (XX) (Figure S1). To explore the conditions under which these precipitants form, we performed xylan synthesis reactions with a serial dilution (0.125−4 mM) of the simplest xylan primer, xylobiose (XX), as an acceptor substrate in the presence of a constant amount of UDP-Xyl (12 mM). Product formation was determined by measuring the optical density at 600 nm (OD_{600}), showing that a ratio of [UDP-Xyl]/[XOS Primer (XX)] above 12 was necessary for substantial aggregate formation (Figure S1).

To further investigate this phenomenon, we performed real-time-nuclear magnetic resonance (RT-NMR) spectroscopy to visualize the chemical landscape of the xylan polymerization reaction over time using XX as the XOS acceptor, with an emphasis on tracking the relative abundances of UDP-Xyl and reducing the internal xylosyl residues (Figure 1b,c). Reactions were carried out in D_2O, and NMR spectra were collected every 15 min over the course of the reaction. We selected representative signals for each reaction component; the H1 signals of the reducing β-xylose (from the xylobiose primer/acceptor, δ 4.58), the internal β-1,4-D-xylose (the product of *Kf*XYS1 chain elongation, δ 4.48), and the α-xylose of UDP-Xyl (nucleotide sugar donor, δ 5.55). Integrals of these signals at each time point were taken and plotted relative to the maximum value of each signal (Figure 1c). We observed that the signals corresponding to the internal β-1,4-D-xylose (δ 4.48), which is near absent at time $t = 0$, increased monotonically until reaching an apex, followed by a rapid decrease. We hypothesize that the decrease in signal intensity is a result of insoluble product

https://doi.org/10.1021/acsmaterialsau.2c00006
ACS Mater. Au 2022, 2, 440−452

formation, rendering the aggregated polymers unobservable via ^{1}H NMR. Signals corresponding to H1 of the reducing β-xylose (δ 4.58), which can arise only from the xylobiose primer, remained relatively constant until approximately the time when the signal for the internal β-1,4-xylose began to decrease and then both signals fell in unison. Signals corresponding to H1 of the nucleotide sugar donor UDP-Xyl decrease monotonically until only ∼35% of the starting area remains, and the signals for internal and reducing xylose of the xylan polymer begin to decrease. After the precipitation event, the rate of UDP-Xyl consumption is greatly diminished and appeared to level off when relatively little soluble acceptor substrate remains available for further transfer.

Synthesis of Xylan Microstructures with Different Primers

Next, we sought to assess the acceptor substrate selectivity of *Kf*XYS1 and determine the range of XOS that could be utilized as acceptors for xylan polymerization. First, *Kf*XYS1 was incubated with 3 mM UDP-Xyl and four structurally distinct saccharide acceptors/primers: β-D-Xylp-(1 → 4)-D-Xylp (XX or xylobiose); β-D-Xylp-(1 → 4)-[4-*O*-Me-α-D-GlcpA-(1 → 2)]-β-D-Xylp-(1 → 4)-D-Xylp (XUX); β-D-Xylp-(1 → 4)-[α-L-Araf-(1 → 3)]-β-D-Xylp-(1 → 4)-β-D-Xylp-(1 → 4)-D-Xylp (XAXX); and 4-*O*-Me-α-D-GlcpA-(1 → 2)-β-D-Xylp-(1 → 4)-β-D-Xylp-(1 → 4)-D-Xylp (UXX) (Figures 2 and S3). Following a 3 h incubation period, the reaction products were analyzed by matrix-assisted laser desorption/ionization time-of-flight mass spectrometry (MALDI-TOF MS). Compared to controls lacking enzyme, reactions containing XX, XUX, and XAXX displayed masses corresponding to successive additions of pentosyl residues (+132 Da) to the XOS primers, while UXX did not appear to be utilized as a substrate by *Kf*XYS1 (Figure S2).

We aimed to determine the effects of primer structure on the ability of xylan to form the previously observed colloidal precipitants. To accomplish this, we prepared xylan synthase reactions to extend XX, XUX, UXX, XAXX, or XX/XUX mixtures in reactions containing 12 mM of xylosyl donors and a final concentration of 0.5 mM acceptor. These assays were monitored by measuring OD_{600} at 10 min time intervals over 24 h. Experimental controls included reactions containing all components except for the acceptor XOS primer and a reaction containing XX and an endo-xylanase (M1), which is expected to cleave any polymeric xylan reaction products formed by the enzyme. The results of this analysis (Figure S3) demonstrated that the rate of insoluble product formation is dependent upon primer structure, with XUX rapidly generating products and XAXX primers yielding a relatively slow formation of less abundant xylan aggregates. Reactions containing equimolar amounts of XX and XUX resulted in final OD_{600} values that fell between the values for XX and XUX alone. In addition, reactions using UXX as the XOS primer or containing XX along with an endo-xylanase resulted in little to no insoluble xylan formation.

Morphology of the Insoluble Xylan Products

The structures of the insoluble xylan products produced using different primer types and combinations were assessed by optical microscopy. Strikingly, it was found that the products formed from XX primers self-assembled into regularly sized, ordered hexagonal microstructures (Figure S4a). Furthermore, many of the microstructures appeared to contain a depression or cavity at the center of the hexagonal face. To determine if these structures contained crystalline domains, the birefringence of the samples was assessed by visualizing them under cross-polarized light (Figure S4b). Observing the microstructures from points in the same plane as the hexagonal face produced a pronounced birefringent effect, while microstructures observed from points on lines normal to the hexagonal face exhibited only mild birefringence. From these results, we concluded that the structures were likely ordered and possessed some degree of crystallinity.

The size and morphology of the biocatalytically synthesized microstructures were examined using scanning electron microscopy (SEM) (Figure 2). XX-type structures (Figure 2a,b) are composed of laminar stacked hexagonal plates joined at the center. Some structures appeared to contain a small hole or indentation in the center of the hexagon, producing a dumbbell shape when viewed from points in the same plane as the hexagonal face. These shapes measured on average 4.99 μm (n = 244, standard deviation (SD) = 0.65 μm) across the hexagonal face under standard conditions (Figures 3b and S5). In contrast, XUX-type microstructures were smaller (diameter = 2.18 μm, n = 379, SD = 0.52 μm) and morphologically distinct from those produced with unsubstituted XOS (Figures 2c,d and 3b). The XUX-type products, while still appearing to contain some degree of crystalline order, as observed by birefringence (Figure S4c,d), lacked the distinct hexagonal morphology observed in XX-type structures. Instead, XUX-type microparticles appeared as biconcave disks with a slightly flattened center. XUX-type microstructures were prone to aggregation after drying in preparation for SEM. To our surprise, the microparticles produced from the combination of XX/XUX primers in the same reaction were morphologically distinct from either of the microstructures formed when using XX or XUX alone (Figure 2e,f). These structures typically contained a vaguely hexagonal base structure with finlike lobes extending from the opposite faces of the hexagon. Interestingly, when reactions were carried out with XAXX XOS primers (XAXX-type), very few insoluble xylan products were generated (Figure 2g,h). The microstructures that did form were vaguely circular and appeared to be deposited in a matrix of unordered, aggregate-like debris, potentially from random aggregation of the saccharide products during synthesis. We chose to forgo diameter measurements on XX/XUX-type and XAXX-type particles due to the heterogeneity of the microstructures preventing an unbiased assignment of what would constitute a diameter.

To further investigate the factors that may influence microparticle morphology, we performed *Kf*XYS1-mediated xylan polymerization using XX as the XOS primer in a broad range of conditions, varying single components of the reaction such as the concentrations of *Kf*XYS1, XX, and UDP-Xyl, and the temperature at which the reactions were performed. We then assessed particle morphology by SEM (Figures S6 and S7). We found that varying concentrations of reaction components or reaction temperatures can result in often subtle yet appreciable differences in the morphologies of the xylan microparticles formed. Notably, reactions at lower temperatures and often at lower substrate concentrations produced microparticles with finlike lobes similar to those formed when using a combination of XX and XUX XOS primers, suggesting that reaction kinetics may play a role in determining the morphologies of enzymatically prepared microparticles.

Dynamic light scattering (DLS) was used to determine the average hydrodynamic diameter of the XX, XUX, and XX/XUX microparticle types (Figures 3c and S8 and Table S1). Because the microparticles do not always remain buoyant and settle to the bottom of solutions over time, we measured the size at two

https://doi.org/10.1021/acsmaterialsau.2c00006
ACS Mater. Au 2022, 2, 440−452

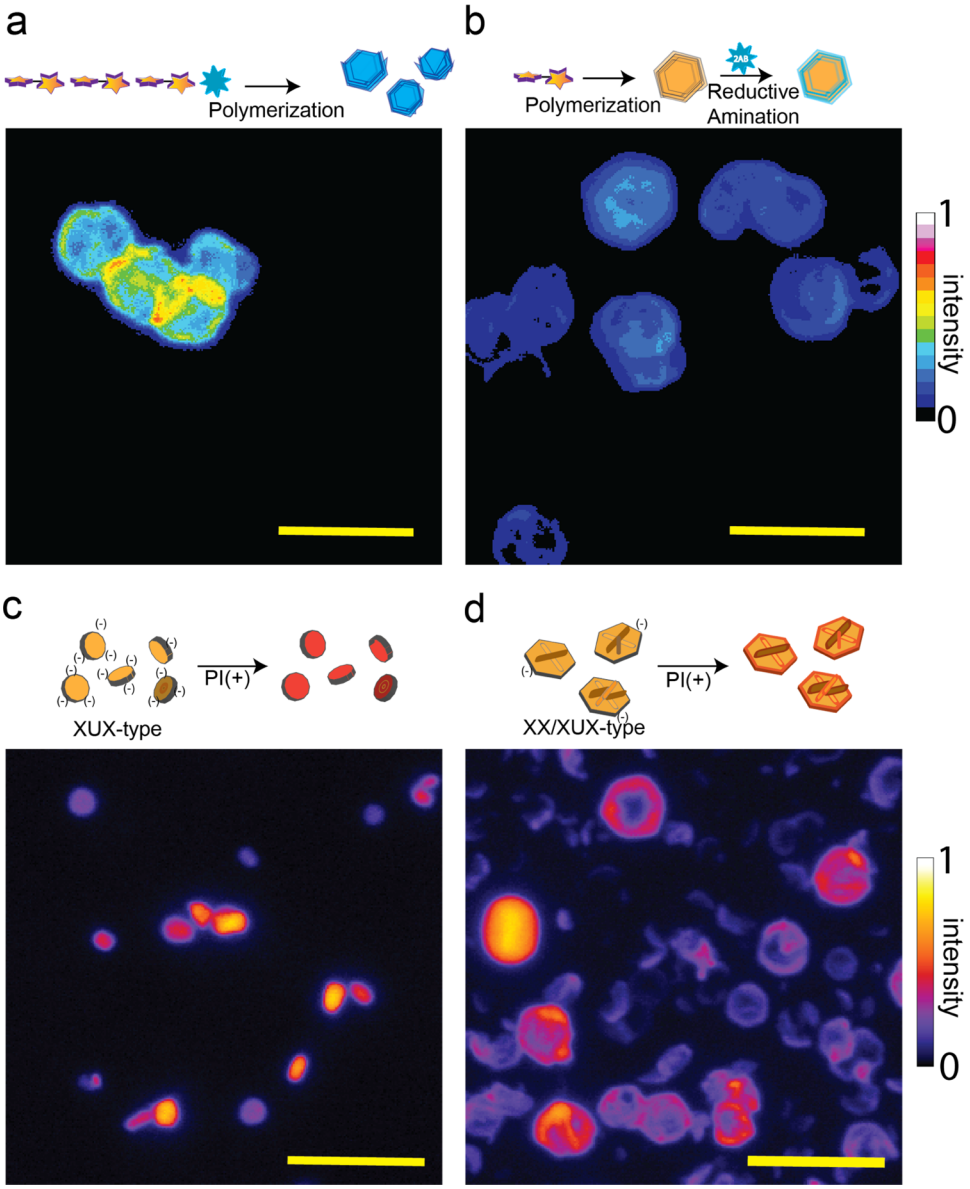

Figure 4. Confocal microscopy of labeled xylan microparticles. (a) Representative images of xylan microparticles produced from the conjugation of the fluorescent tag 2AB to XOS primer reducing ends prior to elongation with *Kf*XYS1. (b) Representative images of XX-type microparticles labeled with 2AB after aggregation. (c) Representative images of XUX-type microparticles stained with the fluorescent dye propidium iodide, which binds to negative charges. (d) Representative images of XX/XUX-type microparticles stained with propidium iodide. Scale bars represent 10 μm.

different time points. We found an average hydrodynamic diameter for all three microparticle types to be approximately 3 μm; however, it appeared that the distribution of microstructure sizes varied between types. Furthermore, the rate at which the particles settled at rest differed between microparticle types (Figures 3c and S8). It should be noted that DLS analysis was conducted assuming a spherical object, and thus, this assumption may somewhat bias the results when considering the irregular shapes exhibited by these microstructures. Nevertheless, the distribution of product sizes of each microstructure-type size is consistent between measurements obtained by DLS or SEM imaging.

Degree of Polymerization (DP) of Soluble and Aggregated Biocatalytically Synthesized Xylans

We hypothesized that the lengths of xylan polymers present within the xylan microparticles might be significantly larger than those polymers that may remain in solution following in vitro xylan polymerization. To investigate this, we utilized MALDI-TOF MS to assess the degree of polymerization of the insoluble versus soluble reaction products (Figure 3a). We allowed xylan aggregation reactions for all XOS primer types (excluding UXX) to continue for 24 h, pelleted the insoluble reaction products, and then sampled the soluble xylan present in the supernatant. The insoluble products were carefully washed by the repeated addition of water followed by pelleting and removal of the supernatant and then dissolved by boiling at 100 °C for 10 min. We examined the size distributions of the products using MALDI-TOF MS, which provided a parameter specifying the DP of the most abundant (DP_{ma}) product in each mixture. This parameter is closely related to, but not identical to, the average DP of the polymers in the mixture. The DP_{ma} of xylans synthesized using XX primers was 14 for nonaggregated xylan polymers remaining in the supernatant of reactions, while the DP_{ma} of redissolved xylan aggregates was 18. Similarly, soluble

https://doi.org/10.1021/acsmaterialsau.2c00006
ACS Mater. Au 2022, 2, 440−452

and aggregated xylan chains generated using XUX primers had DP_{ma} values of 13 and 25, respectively. For XAXX-type reactions, polymers left in the supernatant were found to have a DP_{ma} of 24, while the DP_{ma} of redissolved, aggregate-like debris was 25. Finally, soluble products generated from the XX/XUX primer mixture showed a distribution with a DP_{ma} of 15; however, the masses of all of the observed ions corresponded to polymers containing a single methyl hexuronic acid, suggesting that the peaks arose predominantly from the elongation of the XUX XOS primer. No polymers lacking this MeGlcA were detected in the spectra taken from the supernatant. In contrast, redissolved aggregates displayed two distinct size distributions The most abundant series (DP_{ma} of 19) of ions had masses consistent with unsubstituted xylan polymers, while the other series (DP_{ma} of 22) was consistent with products containing a single MeGlcA substituent. This result suggests that the xylan chain length distributions of soluble and insoluble reaction products were distinct in most cases. However, it is interesting to note that the length distributions for insoluble and soluble xylans do overlap somewhat.

Xylan Microparticles Adopt a Threefold Helical Screw Conformation

To investigate the conformation of enzymatically polymerized xylan polymers that form xylan microparticles, we performed cross-polarized magic-angle spinning solid-state nuclear magnetic resonance spectroscopy (CP-MAS SS NMR) on XX-type and XUX-type structures. From this analysis (Figure 3e), we found the CP-MAS spectra for microstructures prepared with both XOS primer types to be consistent with previously described threefold screw xylans (Figure 3d).[23] To gain further insight into the structural aspects of xylan microparticles, we performed X-ray diffraction (XRD) of the XX, XUX, and XX/XUX microparticle types (Figure S9). The diffraction patterns for all three types were consistent with previously reported spectra describing amorphous xylans prepared via glycosynthase-mediated xylan polymerization.[14]

Functionalization of Xylan Microparticles

We envisioned the microparticles as a potential chassis for drug delivery technologies given the well-documented health benefits of xylans and other hemicelluloses associated with the well-being of the gut microbiome. As such, we designed methods to chemically functionalize these microparticles as proof of concept for their use as drug delivery devices. We chose to pursue two functionalization strategies: labeling primers before *Kf*XYS1-catalyzed elongation and labeling microstructures after formation.

To accomplish the bottom-up synthesis of labeled microparticles, we reductively aminated the reducing terminus of XOS primers using a fluorescent tag, 2-aminobenzamide (2AB), prior to polymer elongation. We then used these labeled substrates as primers for enzymatic synthesis. Microparticles formed from this process appeared smaller than those synthesized using unlabeled primers. Notably, 2AB-labeled microparticles were fluorescent when observed by confocal microscopy under UV light (Figure 4a and Video S1).

We next set out to determine if the reducing ends of the xylan polymers present within the microparticles were accessible after formation. Preformed XX-type microparticles were subjected to a mild reductive amination with 2AB. Following labeling, the microparticles were washed extensively with water and then dissolved at high temperature and analyzed by MALDI-TOF MS, as previously described (Figure S10). The MALDI spectra exclusively included ions with masses corresponding to 2AB-labeled xylans, although this could have been a result of the fact that 2AB-labeled oligosaccharides have a much higher ionization efficiency than unlabeled oligosaccharides during the ionization process, such that unlabeled ions are rarely observed in MALDI spectra of mixtures containing both unlabeled and 2AB-labeled oligosaccharides.[24] In addition, we observed that the DP_{ma} of the postsynthesis 2AB-labeled microstructures (DP_{ma} = 21) appears to be moderately higher than in unlabeled XX-type microstructures. We hypothesize that the mildly reductive labeling procedure may solubilize some shorter xylan chains, artificially shifting the DP_{ma} in the postlabeled structures to appear higher.

We then utilized confocal microscopy to determine areas of the structure most susceptible to reductive amination by this process. *Z*-stacked images revealed a differential fluorescence pattern throughout the xylan microstructures, with a particularly high fluorescence intensity occurring on the edge of the microparticle as well as within the center (Figure 4b and Video S2).

To better understand how the xylan chains assemble to form the microstructures, we treated microparticles prepared with XOS primers that contained the acidic 4-*O*-Me-glucuronosyl substituent with propidium iodide, which is a fluorescent stain that interacts with the negatively charged groups. Each newly formed xylan chain contains one uronic acid residue attached to the xylose next to the reducing end xylose, and this treatment may provide information about the distribution of the uronosyl residues throughout the microparticles. Xylan microparticles prepared from neutral XX primers did not exhibit staining (data not shown); however, those prepared from XUX and mixed XX/XUX XOS primers were effectively labeled (Figure 4c,d), suggesting that the MeGlcA residues present on polymers comprising these microstructures are solvent-exposed. Interestingly, while XUX-type microparticles completely and uniformly stained throughout the entirety of the microstructure, the XX/XUX-type microparticles were labeled primarily in discrete regions, i.e., at the edges of the hexagonal face and to a lesser degree along the lobes of the finlike structures (Figure 4d). This difference in labeling may suggest that XX and XUX XOS primers segregate themselves to distinct areas of the microparticle. This effect may be due, in part, to the association of chemically similar primers or to differences in the chain lengths of the polymers extended from the different primers, causing them to partition to discrete areas of the structures.

Cytotoxicity of Xylan Microparticles

To further the potential of these materials for uses in pharmaceutical or medical pursuits, we endeavored to determine the in vitro toxicity of xylan microparticles on mammalian cells. Cytotoxic effects of XX-type xylan microparticles on a murine cell line (NCTC clone 929 cells) were analyzed using a thiazolyl blue tetrazolium bromide (MTT)-based assay at varying concentrations of XX-type microparticles. We did not observe any toxicity against NCTC clone 929 cells tested when 5, 50 100, or 500 μg/mL of xylan microparticles were added to growth media at time points of 24, 48, and 72 h (Figure S11).

Enzymatic Hydrolysis of Xylan Microparticles

In a previous report, xylan microparticles produced from the extensive hydrothermal treatment of biomass-derived xylans exhibited limited susceptibility to enzymatic degradation by glycoside hydrolases; however, after long incubations, the effects of hydrolysis could be observed at microparticle edges.[16] Thus,

https://doi.org/10.1021/acsmaterialsau.2c00006
ACS Mater. Au 2022, 2, 440−452

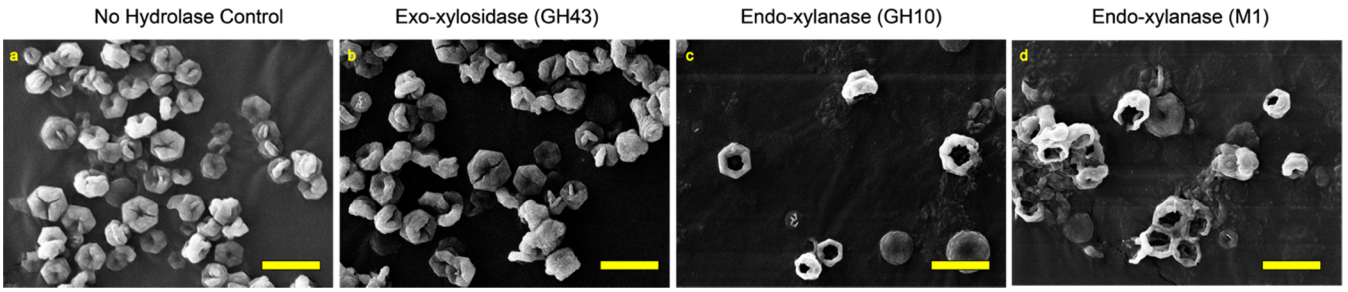

Figure 5. Susceptibility of xylan microparticles to enzymatic hydrolysis. (a–d) Representative SEM images of XX-type microparticles after 48 h incubation with different xylan-active hydrolases. Scale bars represent 10 μm.

we set out to determine if the *Kf*XYS-synthesized xylan microparticles were susceptible to enzymatic hydrolysis by xylanolytic enzymes. XX- and XUX-type microparticles were treated with commercially available xylanases and xylosidases. Three different xylanase treatments were chosen: an exo-β-xylosidase from glycoside hydrolase family 43 (GH43), which acts at the nonreducing end of a xylan chain, an endo-acting xylanase from family GH10, and an endo-acting fungal xylanase from family GH11 (M1). Changes in particle size and morphology after incubation with the enzymes were observed by SEM. XUX-type microstructures displayed little to no discernible changes in size or shape following treatment with all three xylanases (Figure S12). Although XX-type aggregates exhibited no notable structural changes following incubation with the exo-acting β-xylosidase, incubation with endo-xylanases from both GH10 and GH11 resulted in a change in microparticle morphology when compared to control reactions (Figure 5). Specifically, the endo-xylanase-treated XX-type microparticles differed by the formation of large holes in the middle of the hexagonal plates resulting in the generation of microstructures with a hollow core, reminiscent of a hex-nut (Figure 5c,d). It should be noted that many of the XX-type microparticles contained a small hole at the center prior to the addition of enzyme; however, a stark difference in the hole size is apparent after enzyme treatment. Most of the microstructures in the preparation were converted to this hex-nut form by the endo-xylanase; however, we observed some variability such as microstructures that had rounded edges and lacked holes in their centers. The susceptibility to enzymatic hydrolysis, or lack thereof, may imply that the xylan chains assemble into multiple distinct structural types with varying degrees of enzyme accessibility within a given macrostructure.

Discussion

The present study reports the development of an enzymatic platform to generate pure xylan polymers with controlled fine structural features by harnessing the action of an ancestral xylan synthase, *Kf*XYS1. In addition, we show that by optimizing reaction conditions, we can synthesize xylan polymers that self-assemble into morphologically distinct microparticles that adopt a threefold helical screw conformation and whose final form could be easily controlled by varying just a single sugar on the saccharide primer. The threefold helical screw conformation, with one 360° turn per three glycosidic bonds, is the most stable structure for xylan in solution.[25] Previous works exploring routes of xylan synthesis in vitro have typically employed chemical or chemienzymatic methods for the polymerization of the xylan backbone, which are expensive and require difficult-to-obtain reagents and equipment.[14] These methods have proved invaluable for the study of xylans and polymer–polymer interactions; however, in contrast to the platform described here, they lack the ability to fully recapitulate and improve understanding of polysaccharide synthesis pathways in natural systems. One key issue with studying plant polysaccharide biosynthesis is that many enzymes show a preference for higher DP acceptor substrates, which in the case of xylan can become difficult because of solubility issues. We envision that the cell-free biocatalytic synthesis employed here will serve as a base, enabling platform that can be expanded upon with the addition of other polymer-modifying enzymes, such as the branching glycosyl and acetyl transferases that decorate xylan polymers in vivo. Indeed, we have recently described the use of *Kf*XYS1 in combination with a series of rationally engineered xylan *O*-acetyl transferases (XOATs) to synthesize acetylated xylan polymers in a one-pot reaction.[26] In the future, we speculate that in vitro platforms like this will allow researchers to more rapidly engineer enzymes like XOATs for in planta gene replacement to produce plant cell walls with tuned properties. Future work will focus on the incorporation of auxiliary enzymes such as these into the in vitro xylan synthesis platform, with a promise to reveal intricacies of enzyme function and behavior that govern the synthesis of the ornately decorated polymers synthesized within the Golgi bodies of live plants.

Phylogenetic evidence suggests that *Kf*XYS1 represents one of the earliest known examples of xylan biosynthetic activity and is ancestral to the enzymes that function to synthesize the xylans found in all terrestrial plants today.[12] One critical and notable aspect of *Kf*XYS1 to the experiments presented here is that it remains capable of efficient xylan polymer elongation in the presence of millimolar levels of UDP, a byproduct of the glycosyltransferase reaction. *Kf*XYS1 proved to be unrivaled in xylan synthesis capabilities when compared to xylan synthases cloned from more evolved plant lineages[12] (unpublished results). In addition, we show that *Kf*XYS1 is promiscuous in terms of the structure of the saccharide primer as evidenced by the ability to readily utilize primers containing different side-chain structures, including those substituted with a 2′-linked 4-*O*-methyl-glucuronosyl residue (XUX), a 3′ arabinosyl substituent (XAXX), and a labeled reducing terminus (X6-2AB). In contrast, UXX could not be extended by *Kf*XYS1, which is likely a result of steric constraints presented by the 4-*O*-methyl-glucuronosyl substituent at *O*-2″ of the nonreducing terminal xylose residue, the residue to which xylose is transferred by *Kf*XYS1.

Perhaps, the most surprising and intriguing finding from this study is that *Kf*XYS1 polymerization reactions with suitable quantities of donor and acceptor substrates can lead to the formation of ordered microstructures and that their morphologies could be manipulated based on the XOS primer structure. One aspect of this work that is difficult to reconcile is that the

https://doi.org/10.1021/acsmaterialsau.2c00006
ACS Mater. Au 2022, 2, 440–452

xylan microparticles produced here were found to produce a birefringent effect when viewed through cross-polarized lenses, suggesting some degree of order within the structures (Figure S4). However, XRD analysis of XX- and XUX-type particles seemed to contradict this finding and suggests that these microparticles are predominantly comprised of amorphous xylan aggregates (Figure S9). We intend to further probe the arrangement and packing of xylan chains within these enzymatically synthesized products in future work to better understand how the combined data can provide insight into the molecular architecture.

Previous work has demonstrated the enzymatic synthesis of other cell wall polysaccharides, which can form aggregates, with relevant examples including the glycosynthase-mediated synthesis of crystalline β-D-(1,3)(1,4) glucans,[27] as well as the synthesis of large-molecular-weight xyloglucan polymers lacking galactosylation, which were found to form insoluble products.[28] Furthermore, Kobayashi et al. described the enzymatic synthesis of xylan polymers using cellulase as a catalyst and reported the formation of a white xylan precipitant that produced CP-MAS spectra very similar to those described in this work.[13] In addition, the xylans produced in the study by Kobayashi et al. were reported to have an average degree of polymerization of around 23 xylosyl units, suggesting that these polymers and insoluble products may be very similar to those that we have produced in this work.[13] Reports of crystalline xylans first emerged in the 1940s that described the formation of laminar hexagonal microcrystals that assemble from short-chain xylan fragments generated by autoclaving plant biomass and possess an unmistakable resemblance to the microparticles synthesized within this work (Figure 2a,b).[15,16,18] Here, we have generated diverse microstructures de novo via enzymatic polymerization, granting us greater control of the polymer structures participating in polymer aggregation and the morphologies of microstructures produced when compared to previously described methods of xylan microparticle preparation.

We anticipate that many other unexplored structures may serve as XOS primers, and we propose that a greater diversity of microparticle morphologies may be achievable. We hope to further explore this possibility in future studies, as well as investigate other ways to influence xylan synthesis and self-assembly, perhaps via side-chain addition or the controlled mixing of multiple XOS primer types in a single xylan synthesis reaction. Further analysis is also warranted into the mixing of xylan primers at different points or lengths of polymerization, essentially giving certain polymers a "head-start" in elongation before adding others. In this way, it may be possible to synthesize cores of one XOS-type while then decorating or modifying these cores with polymers containing other modifications or functionalities. Although here we have described a new biocatalytic platform to create xylan microstructures completely comprised of xylans, there is also potential to enzymatically incorporate other polymers and components into composite particles. We hope to develop this platform to synthesize xylans in the presence of cellulosic materials such as nano- or microcrystalline cellulose preparations, as a green technology for cellulose labeling. Further investigations into this arena promise to develop the understanding of xylan synthesis and xylan/cellulose interactions as well as aid in the construction of biobased materials, which could mimic the plant cell wall in terms of complexity, plasticity, and biocompatibility.

In this study, we have described several examples and insights into how this technology might be utilized, focusing specifically on biomedical applications given the well-established biocompatibility of xylans. For this reason, we tested the biocompatibility and degradability of XX-type microparticles and found their characteristics to be fully in line with what we would expect of unassociated xylans. In addition, the ability to modify xylan microstructures, either ionically or covalently, bodes well for the implementation of these structures as biologically inspired drug delivery chassis. Given these results, we believe that xylan microparticles may have commercial potential in the pharmaceutical or nutritional industries. Though many hurdles lie in the way of scale-up and mass production of xylan microparticles through enzymatic synthesis, chiefly the high cost of the donor substrate UDP-Xyl, the tantalizing prospect of fully simulating natural pathways for synthesis is rapidly approaching reality. One-pot multienzyme approaches potentially reduce both the complexity and cost of in vitro carbohydrate synthesis compared to current chemical methods and have therefore gained attention in the past decade. Many of these studies involve carbohydrate polymerization by glycosyltransferases coupled with substrate regeneration pathways, which support in vitro synthesis by exchanging kinetically unfavorable byproducts for activated substrates. This strategy promotes enhanced yield and lowers the required amount of starting donor substrates. These principles have been successfully utilized for in vitro synthesis of N-glycans, but to the best of our knowledge, these have not been applied to plant polysaccharides.[29,30] The platform we have presented here is a candidate for such systems, primarily as a mechanism to reduce the cost of UDP-xylose. We expect these technologies to mature rapidly as the understanding of plant cell wall biosynthetic and metabolic pathways advances.

CONCLUSIONS

Here, we have described the enzymatic synthesis and self-assembly of xylan microparticles with morphologies that can be tuned based on fine structural features of the saccharide primers used to initiate polymerization. We have investigated the conditions under which xylan microparticles are formed, the lengths and conformations of the polymers that comprise the particles, as well as the ability to modify the structures using chemical probes and hydrolytic enzymes. Taken together, we present a novel biocatalytic route to xylan-based materials, which we envision to have many potential uses in industries that require bioderived or biocompatible products.

METHODS

Reagents

All chemicals were purchased from VWR International unless otherwise indicated. β-D-Xylp-(1 → 4)-D-Xylp (XX i.e., xylobiose), β-D-Xylp-(1 → 4)-[4-*O*-Me-α-D-GlcpA-(1 → 2)]-β-D-Xylp-(1 → 4)-D-Xylp (XUX), β-D-Xylp-(1 → 4)-[α-L-Araf-(1 → 3)]-β-D-Xylp-(1 → 4)-β-D-Xylp-(1 → 4)-D-Xylp (XAXX), and 4-*O*-Me-α-D-GlcpA-(1 → 2)-β-D-Xylp-(1 → 4)-β-D-Xylp-(1 → 4)-D-Xylp (UXX)) were purchased from Megazyme International (Ireland).

Cloning and Expression of *Kf*XYS1

*Kf*XYS1 was cloned into the pGEn2-DEST mammalian expression vector[31] and expressed in human embryonic kidney cells, as previously described by Jensen et al.[12] The expression construct (His-GFP-*Kf*XYS1) used in this work encodes a fusion protein comprising an amino-terminal signal sequence, an 8xHis tag, an AviTag recognition site, the "superfolder" GFP (sfGFP) coding region, the recognition sequence of TEV protease, and residues 27−445 of *Kf*XYS1. Recombinant expression and purification were performed by transient

https://doi.org/10.1021/acsmaterialsau.2c00006
ACS Mater. Au 2022, 2, 440−452

transfection of suspension culture HEK293-F cells with pGEn2-*Kf*XYS1 and a HisTrap HP 1 mL column (GE Healthcare, Little Chalfont, U.K.), as previously described.[11,12] His-GFP-*Kf*XYS1 was concentrated to >1 mg/mL using an Amicon Ultra Centrifugal Filter Device (30,000 molecular weight cut-off (MWCO); Merck Millipore) and dialyzed (3,500 MWCO) into *N*-(2-hydroxyethyl)piperazine-*N*′-ethanesulfonic acid (HEPES) sodium salt−HCl (50 mM, pH 7.4) and used directly for reactions or stored at 4 or −80 °C. The purified fusion protein used throughout the experiments herein will be referred to as *Kf*XYS1 for simplicity.

Production of UDP-Xylose

UDP-xylose (UDP-Xyl) was synthesized from UDP-glucuronic acid (UDP-GlcA, Carbosynth) via a recombinant human UDP-xylose synthase (hUXS). hUXS was previously cloned into the pET15b vector and transfected into *Escherichia coli* for expression.[32] This construct was obtained through a generous gift from Dr. Zachary Wood (UGA), plated onto an LB-agarose plate containing ampicillin (100 μg/mL) as a selection marker, and grown at 37 °C for 16 h. Single colonies were used to inoculate 5 mL starter cultures of LB broth with ampicillin (100 μg/mL), and the cultures were grown for 16 h with shaking at 200 rpm. These cultures were then used to inoculate 6, 1 L cultures of LB broth containing ampicillin (100 μg/mL). The cultures were shaken at 37 °C, 200 rpm until reaching an OD_{600} of 0.6 as measured by a spectrophotometer, at which point the hUXS expression was induced with the addition of 0.2 mM isopropyl β-D-1-thiogalactopyranoside (IPTG). Protein expression was continued for 3.5−6 h at 37 °C, at which point the cultures were centrifuged at 5,000*g* for 15 min, the supernatant was removed, and the pellets were stored at −20 °C.

The cell pellets were resuspended in a total of 90 mL of buffer A (50 mM HEPES pH 7.4, 0.4 M NaCl, and 20 mM imidazole) and subjected to lysis with two successive phases on a French press. The slurry was transferred to conical centrifuge tubes, and the cell debris was separated by centrifugation at 12,000*g* for 30 min. The supernatant was collected, diluted to 300 mL in buffer A, and filtered via a 5 μm vacuum filtration device (Millipore). This mixture was then loaded at a rate of 5 mL/min onto a 5 mL HisTrap HP (GE scientific) pre-equilibrated with buffer A using an ÄKTA pure 25 L chromatography system. After loading, the column was washed and eluted with a step gradient, consisting of five CVs per condition of buffer A to buffer B (50 mM HEPES pH 7.4, 0.4 M NaCl, 500 mM imidazole) at a flow rate of 5 mL/min consisting of 20, 60, and 100% buffer B. Fractions containing peaks as observed by UV absorbance were analyzed by sodium dodecyl sulfate-polyacrylamide gel electrophoresis (SDS-PAGE) and those containing the protein of interest were pooled and dialyzed into 50 mM Tris−HCL pH 8 with 250 mM NaCl and 10 mM ethylenediaminetetraacetic acid (EDTA) for 16 h at 4 °C.

UDP-Xyl was then synthesized from UDP-GlcA by preparing reactions containing 40 μM hUXS, 30 mM UDP-glucuronic acid disodium salt (Carbosynth), 10 mM dithiothreitol (DTT) in 50 mM Tris−HCl buffer pH 8 with 10 mM EDTA. Reactions were incubated at 37 °C with shaking at 200 rpm for 48 h. Nucleotide sugar products were then separated from hUXS via diafiltration using a Vivacell 70 ultrafiltration concentrator (10 kD MWCO; Satorius AG) by centrifugation at 3,800*g* for 4 h at 4 °C. The filtrate was diluted 1:20 into an anion-exchange (AnEx) buffer A comprised of 20 mM ammonium acetate (pH 4.8) and loaded in 40 mg batches onto a 5 mL HiTrap Q HP anion-exchange chromatography column (GE Scientific) pre-equilibrated with 10 CV of ammonium acetate (pH 4.8), using an ÄKTA pure 25 L chromatography system at a rate of 5 mL/min. The column was washed and eluted with a step gradient, consisting of five CVs per condition of AnEx buffer A to AnEx buffer B (0.5 M ammonium acetate pH 4.8). These consisted of two sequential steps of 40 and 100% AnEx buffer B. Peaks eluted by 40% AnEx buffer B containing the purified UDP-Xyl were collected, diluted 1:10 in water, and lyophilized. The dry materials were then resuspended in 20 mL of water, repeatedly frozen, and lyophilized until ammonium acetate was nearly removed (~3 times). Combined fractions were resuspended in water, and their UDP-Xyl content was quantified by measuring the absorbance at 262 nm read with a Take 3 plate (Biotek) and a Biotek Synergy LX multimode plate reader (BioTek Instruments). Measurements were compared to a standard curve prepared from the known molarity of UDP-GlcA disodium salt in water. Purified UDP-Xyl was diluted to a final concentration of 120 mM and stored at −20 °C in aliquots until use.

*Kf*XYS1 Oligosaccharide Primer Screen

Reactions were prepared containing 0.5 μM *Kf*XYS1, 3 mM UDP-Xyl, 50 mM HEPES sodium salt pH 7.3, 0.5 mM of oligosaccharide primer xylobiose (XX), 2′-(4-*O*-methyl-α-D-glucuronosyl)-xylotriose (XUX), 3″-arabinofuranosyl-xylotetraose (XAXX), and 3″-(4-*O*-methyl-α-D-glucuronosyl)-xylotriose (UXX) at various concentrations (0.5, 0.25, 0.125, 0 mM). Prior to the addition of UDP-Xyl, 2 μL of the reaction mixture was removed and mixed with Dowex 50W slurry and incubated for 1 h at room temperature (RT). Following the addition of UDP-Xyl, reactions were allowed to incubate at RT for 1 h, at which time 2 μL was removed and mixed with 10 μL of Dowex 50W anion-exchange resin and incubated for 12 h at RT. The samples along with the no UDP-Xyl controls were pelleted, and 2 μL of the supernatant was mixed with 2 μL of 2,5-dihydroxybenzoic acid (DHB) (Sigma-Aldrich) dissolved at a concentration of 20 mg/mL in 50% aqueous methanol on a Bruker MALDI-TOF MS target plate and allowed to dry. The samples were analyzed with an LT Bruker LT Microflex spectrometer (Bruker, Billerica, MA), as described previously.[11] Positive-ion spectra were recorded with a minimum of 200 laser shots summed to generate each spectrum.

Monitoring the Synthesis and Formation of Insoluble Xylan Products

Enzyme reactions containing 0.5 μM *Kf*XYS1, 12 mM UDP-Xyl, 50 mM HEPES sodium salt pH 7.3, and 0.5 mM acceptor oligosaccharide primers (XX, XUX, XAXX, UXX) or 25 mM each of XX and XUX were prepared. A control reaction containing 10 ng M1 xylanase (Megazyme Ireland) was added to xylobiose primed reactions as a control. Reactions were performed in triplicate in a Costar clear 96-well plate (Corning). Reactions were then monitored by measuring the OD_{600} using a Biotek Synergy LX multimode plate reader every 5 min for 24 h.

RT-NMR Analysis of Xylan Microparticle Formation

*Kf*XYS1 was dialyzed for 36 h into 50 mM sodium phosphate buffer pH 7.3 prepared in 99% deuterium oxide (D_2O). Stock solutions of UDP-Xyl and xylobiose and buffer were prepared in D_2O. A 200 μL reaction was prepared on ice comprised of 0.88 μM *Kf*XYS1, 20 mM UDP-Xyl, and 0.5 mM xylobiose in 50 mM sodium phosphate pH 7.3. The reaction was gently vortexed and then quickly transferred to a 3 mm glass NMR tube. The 1D ^1H spectra were recorded every 15 min with a sample temperature of 25 °C on a Varian Inova NMR spectrometer operating at 600 MHz and equipped with a 5 mm cold probe (Agilent, Santa Clara, CA). Chemical shifts were measured relative to internal DMSO (δ ^1H 2.721). The NMR spectra were processed using MestReNova software (Mestrelab Research S.L., Santiago de Compostela, Spain).

Scale-Up of Microparticle Production for Structural Analysis

For the large-scale production of xylan microparticles, reaction mixtures containing 0.5 μM *Kf*XYS1, 12 mM UDP-Xyl, and 0.5 mM xylan oligosaccharide primer (XX, XUX, XX/XUX) were prepared in 50 mM HEPES sodium salt−HCl pH 7.3. For the reactions with XX/XUX primer mixtures, a concentration of 0.25 mM of each primer type was used to reach a final concentration of 0.5 mM oligosaccharide primer. The total reaction volume for each substrate type was 22.5 mL, split equally between three 15 mL conical tubes. Xylan polymerization was allowed to progress for 24 h, at which point all insoluble materials were pelleted via centrifugation at 2,800*g* for 5 min, and the supernatant was removed and placed in a fresh tube, with a small aliquot (20 μL) of the supernatant stored at −20 °C for further analysis. The pellets were washed with 5 mL of sterile, cell culture grade water (Corning) and pelleted again at 2,800*g*. This process was repeated five times. Finally, the microparticles were suspended in 20% aqueous ethanol and stored at room temperature for later use.

https://doi.org/10.1021/acsmaterialsau.2c00006
ACS Mater. Au 2022, 2, 440−452

Magic-Angle Spinning Solid-State NMR of Xylan Microparticles

Approximately 12 mg of xylan microstructures (XX- or XUX-type) suspended in 20% aqueous ethanol were spun at 2,800*g* and washed 3× with deionized H_2O and then washed 3× consecutively with 99% D_2O (Cambridge Isotope Laboratory Inc.). The microparticles were then resuspended in 0.2 mL of D_2O by pipetting and packed into a 30 μL HR-MAS-disposable-insert (Bruker), which was placed in a 1.5 mL Eppendorf tube, and gently spun at 3,000*g* for 30 s. The excess D_2O (supernatant) was then removed without disturbing the packed microparticles, and the process was repeated until the insert was completely filled with xylan microparticles while minimizing the amount of D_2O in the insert. The CP-MAS NMR spectra were recorded using a Bruker Advance Neo 600 MHz spectrometer equipped with a 4 mm CmP-HR-MAS probe with a sample temperature of 25 °C and a spinning speed of 10 kHz.

MALDI-TOF Mass Spectrometry of Xylan Polymers

For analysis of the reaction mixture supernatant, samples were pelleted at indicated times at 2,800*g* for 5 min. A 10 μL aliquot of the reaction was taken from the top without disturbing the pelleted microparticles, mixed with 10 μL of dH_2O and 5 μL of Dowex 50W anion-exchange resin, and incubated for at least 30 min. Samples were then centrifuged to pellet the resin, and 2 μL of the supernatant was mixed with 2 μL of 2,5-dihydroxybenzoic acid (DHB, Sigma-Aldrich, 20 mg/mL in 50% aqueous methanol) on a Bruker MALDI-TOF MS target plate and allowed to dry. The samples were analyzed with an LT Bruker LT Microflex spectrometer (Bruker, Billerica, MA), as described previously.[11] Positive-ion spectra were recorded with a minimum of 200 laser shots summed to generate each spectrum.

To analyze insoluble xylan polymers, the xylan microparticles were gently suspended by pipetting, and 10 μL of the colloidal solution was then removed and placed in strip tubes. The suspension was pelleted by centrifugation at 5,000*g* for 3 min, the supernatant was removed, and 50 μL of dH_2O was added to resuspend the pellet. This washing was repeated five times, at which point the microparticles were left in 50 μL of dH_2O and then heated to 100 °C for 5 min. A 2 μL aliquot was then removed and prepared for analysis by MALDI-TOF MS in the same manner as described for soluble polymers.

Light Microscopy

Xylan microparticles were gently resuspended by pipetting, and 3 μL of the colloidal slurry was removed, mixed with an equal volume of glycerol, and placed on a glass microscopic slide (colorfrost/plus; Fisher Scientific). The sample was then covered with a glass coverslip and immediately observed using a Nikon Eclipse 80i microscope equipped with a Nikon Plan Fluor 40×/0.075 objective. To observe the birefringence of xylan microparticles, a polarizing lens (Olympus, Japan) was placed over the bottom light source of the microscope and a polarizing filter was also included above the objective. The polarizing lens was rotated to produce a dark as possible field of view in the absence of sample. Images were captured using the NIS Elements (4.3) software package.

Dynamic Light Scattering

Xylan microparticles were diluted to 0.1 mg/mL in a storage buffer (20% aqueous ethanol). Scattering was measured at 25 °C in triplicate with a Malvern Zetasizer Nano ZS (Malvern Panalytical). The size of the structures was determined by the weighted average of the percentage of intensity measured at each size across the replicates.

Scanning Electron Microscopy

Thoroughly washed xylan microparticles were resuspended in a dilute colloidal suspension, and 3 μL of the suspension was deposited onto SEM aluminum specimen mounts (Ted Pella Inc.) with a carbon adhesive tab (Electron Microscopy Sciences) attached. The mounts were then allowed to dry in a desiccation chamber for at least 24 h, at which point they were sputter-coated with a thickness of 10 nm (stage height −10 nm) with gold−palladium coating using a Leica EM ACE200 sputter coating system. Following sputtering, the samples were imaged using a Jeol JSM-6010LV scanning electron microscope. Sizes of xylan microparticles were determined by analyzing representative SEM images using ImageJ.[33]

Labeling of Xylan Microparticles

Xylohexaose (Megazyme Ireland) was labeled with the fluorescent dye 2-aminobenzamide (2AB, Sigma-Aldrich), as previously described.[11] Xylohexaose-2AB (0.5 mM) was then incubated with *Kf*XYS1 and 30 mM UDP-Xyl in HEPES sodium salt pH 7.3 for 12 h, before pelleting and washing as described previously. Alternatively, xylan microparticles generated via a large-scale synthesis were labeled with 2AB after formation as follows: 0.2 mg of XX-type microparticles was suspended in 100 μL of 0.5 M sodium cyanoborohydride ($NaCNBH_4$, Sigma-Aldrich) and 0.25 M 2AB (Sigma-Aldrich). Reaction pH was adjusted to between 5 and 5.5 with 1 M acetic acid. The mixture was then incubated at 45 °C for 12 h. Following incubation, the reaction was pelleted by centrifugation at 5,000*g* for 5 min, the supernatant was removed, and the microparticles were washed 10× with 1 mL of dH_2O. Control samples were also prepared following the same procedure but lacking $NaCNBH_4$ in the reaction mixture.

Xylan microparticles (~20 μg) were labeled with propidium iodide by incubation for 30 min in 100 μg/mL aq. propidium iodide (Sigma-Aldrich). Following incubation, the microparticles were pelleted and washed with 50 μL of water. The microparticles were then pelleted again, and the supernatant was removed, before resuspension in 5 μL of 1% agarose solution (60 °C), and mounting on a glass microscopic slide.

Degradation of Xylan Microparticles with Hydrolases

Xylan microparticles (5 mg) stored in water were pelleted by centrifugation at 2,800*g* for 5 min, and the supernatant was removed. The microstructures were resuspended in 2.5 mL of dH_2O and pipetted repeatedly to produce a well-suspended slurry. An aliquot (10 μL) of the slurry was then removed and placed in a 0.2 mL polymerase chain reaction (PCR) strip tube. The suspension was then pelleted at 5,000*g* in a microcentrifuge for 5 min, and the supernatant was removed and replaced with 10 μL of the appropriate buffer. Ammonium acetate (100 mM pH 5) was used for both the GH11 M1 xylanase from *Trichoderma viride* (E-XYTR1, Megazyme Ireland) and GH10 xylanase from *Cellvibrio japonicus* (XYNACJ, Megazyme Ireland), while HEPES sodium salt (100 mM pH 7.4) was used for the exo β-xylosidase from *Bacillus pumilus* (E-BXSEBP, Megazyme Ireland). Enzyme stocks were diluted in water to a concentration of 0.01 mg/mL (0.023, 0.0025, and 0.0018 units for M1, XYNACJ, and E-BXSEBP, respectively), and 10 μL was added to each sample, giving a final concentration of 50 mM buffer, ~20 μg microparticles, and 100 ng enzyme. No enzyme controls were also prepared in ammonium acetate buffer pH 5. Reactions were performed in triplicate and incubated at 37 °C for 24 or 48 h. At each time point, the reaction was gently resuspended by pipetting, and 3 μL was removed, pelleted at 2,800*g* for 5 min, washed repeatedly with dH_2O, and mounted for examination by SEM.

Confocal Microscopy

Labeled and stained microparticles were mounted on a glass slide under a cover glass. Microstructures were imaged as *Z*-stacks on an Olympus Fluoview FV1200 equipped with a 100×/1.40 NA oil immersion objective. The 2AB fluorescent signal was visualized using a 405 nm excitation laser and a band-pass filter of 425−475 nm with an SDM490 dichroic mirror. Propidium iodide fluorescent signal was visualized using a 559 nm excitation laser and a 570−670 nm emission filter. Images were constructed using ImageJ.[33]

X-ray Diffraction

The crystallinity of the xylan microstructures was measured by X-ray diffraction (XRD) using a Rigaku (Tokyo, Japan) Ultima IV diffractometer with a Cu Kα radiation having a wavelength of λ (Kα1) = 0.15406 nm generated at 40 kV and 44 mA. Samples were placed on a quartz substrate, and the diffraction intensities were measured with 2θ in the range of 8−42° using a step size of 0.02° at a rate of 2°/min. Amorphous cotton linters (Amorphous CL) were included as an experiment control.

https://doi.org/10.1021/acsmaterialsau.2c00006
ACS Mater. Au 2022, 2, 440−452

Toxicity Screening of Xylan Microparticles

The toxicity of the xylan microparticles was measured based on the ability of cells with functional mitochondria to reduce the dye thiazolyl blue tetrazolium bromide (MTT, Sigma-Aldrich, M2128) to a blue formazan product that absorbs light at 490 nm. XX-type particles (5 mg) were dissolved in molecular-grade water (1 mL), and serial dilutions were made for each concentration tested. NCTC clone 929 cells (ATCC CCL-1) were seeded in 48-well plates using a total volume of 400 μL. The following day, 77 μL of the media was replaced with 77 μL of xylan microparticles (final concentrations were 5, 50, 100, and 500 μg/mL) or vehicle control in triplicate wells. After 24, 48, and 72 hours, MTT dye was added and the absorbance in each well was read at 490 nm. Post screening, the data was processed using Graphpad Prism version 8.0. For each concentration, the mean blank-corrected absorbance across triplicate wells was calculated and expressed as a fold change relative to the vehicle-treated wells.

Statistics

The mean size of xylan microparticles as calculated by SEM was determined by a two-tailed *t*-test with unequal variance. *P*-value = 8.9959×10^{-204}, degrees of freedom = 621. All representative images are obtained from experiments that included at least two independent experimental replicates unless otherwise indicated in the figure legends.

Experimental Details

No unexpected or unusually high safety hazards were encountered while conducting the experiments laid out within this work.

■ ASSOCIATED CONTENT

Supporting Information

The Supporting Information is available free of charge at https://pubs.acs.org/doi/10.1021/acsmaterialsau.2c00006.

Analysis of xylan microparticle formation conditions by OD_{600} (Figure S1); MALDI-TOF-based screen of *Kf*XYS1 XOS acceptors (Figure S2); rate and formation of xylan microparticles from different XOS acceptors (Figure S3); optical microscopy of XX- and XUX-type microparticles (Figure S4); schematic demonstrating the method of determining XX-type particle diameter (Figure S5); effect of substrate concentration on the XX-type microparticle morphology (Figure S6); effect of temperature and *Kf*XYS1 concentration on the XX-type microparticle morphology (Figure S7); DLS analysis of xylan microparticles (Table S1); DLS analysis of xylan microparticles (Figure S8); XRD analysis of xylan microparticles (Figure S9); MALDI-TOF MS of 2AB-labeled XX-type microparticles (Figure S10); toxicity screen of the XX-type microparticles (Figure S11); SEM of hydrolase digested XUX-type microparticles (Figure S12) (PDF)

Video of *Z*-stacked XX-type microparticles prelabeled with 2AB (Video S1) (AVI)

Video of *Z*-stacked XX-type microparticles postlabeled with 2AB (Video S2) (AVI)

■ AUTHOR INFORMATION

Corresponding Author

Breeanna R. Urbanowicz − *Complex Carbohydrate Research Center, University of Georgia, Athens, Georgia 30602, United States; Department of Biochemistry and Molecular Biology, University of Georgia, Athens, Georgia 30602, United States;* orcid.org/0000-0001-5247-4513; Phone: +1 706-542-4419; Email: breeanna@uga.edu; Fax: +1 706-542-4412

Authors

Peter J. Smith − *Complex Carbohydrate Research Center, University of Georgia, Athens, Georgia 30602, United States; Bioscience Center, National Renewable Energy Laboratory, Golden, Colorado 80401, United States*

Thomas M. Curry − *Complex Carbohydrate Research Center, University of Georgia, Athens, Georgia 30602, United States; Department of Biochemistry and Molecular Biology, University of Georgia, Athens, Georgia 30602, United States*

Jeong-Yeh Yang − *Complex Carbohydrate Research Center, University of Georgia, Athens, Georgia 30602, United States; Department of Biochemistry and Molecular Biology, University of Georgia, Athens, Georgia 30602, United States;* Present Address: Agricultural Research Service, U.S. Department of Agriculture, Athens, Georgia 30605, United States

William J. Barnes − *Complex Carbohydrate Research Center, University of Georgia, Athens, Georgia 30602, United States*

Samantha J. Ziegler − *Bioscience Center, National Renewable Energy Laboratory, Golden, Colorado 80401, United States*

Ashutosh Mittal − *Bioscience Center, National Renewable Energy Laboratory, Golden, Colorado 80401, United States;* orcid.org/0000-0002-0434-0745

Kelley W. Moremen − *Complex Carbohydrate Research Center, University of Georgia, Athens, Georgia 30602, United States; Department of Biochemistry and Molecular Biology, University of Georgia, Athens, Georgia 30602, United States*

William S. York − *Complex Carbohydrate Research Center, University of Georgia, Athens, Georgia 30602, United States*

Yannick J. Bomble − *Bioscience Center, National Renewable Energy Laboratory, Golden, Colorado 80401, United States;* orcid.org/0000-0001-7624-8000

Maria J. Peña − *Complex Carbohydrate Research Center, University of Georgia, Athens, Georgia 30602, United States*

Complete contact information is available at: https://pubs.acs.org/10.1021/acsmaterialsau.2c00006

Author Contributions

P.J.S., M.J.P., J.-Y.Y., Y.J.B., T.M.C., and B.R.U. designed and performed the experiments and analyzed the data. K.W.M. and J.-Y.Y. expressed recombinant proteins in HEK cells. W.J.B. performed the confocal microscopy. S.J.Z. performed the DLS data collection and analysis. A.M. performed the XRD data collection. W.S.Y., M.J.P., K.W.M., Y.J.B., and B.R.U. designed the experiments, analyzed and interpreted the data, and edited the manuscript. P.J.S., Y.J.B., M.J.P., and B.R.U. wrote the manuscript. W.S.Y., M.J.P., and B.R.U. conceived and led the project. All authors read and revised the manuscript.

Notes

The authors declare no competing financial interest.
The data that supports the findings of this study are available from the corresponding author.

■ ACKNOWLEDGMENTS

Funding was provided by the Center for Bioenergy Innovation (CBI), a U.S. Department of Energy Bioenergy Research Center supported by the Office of Biological, Environmental Research in the DOE Office of Science and National Institutes of Health (P41GM103390 and R01GM130915). This work was authored, in part, by Alliance for Sustainable Energy, LLC, the manager and operator of the National Renewable Energy Laboratory for the U.S. Department of Energy (DOE) under Contract No. DE-

AC36-08GO28308. The views expressed in the article do not necessarily represent the views of the DOE or the U.S. Government. The U.S. Government retains and the publisher, by accepting the article for publication, acknowledges that the U.S. Government retains a nonexclusive, paid-up, irrevocable, worldwide license to publish or reproduce the published form of this work, or allow others to do so, for U.S. Government purposes.

REFERENCES

(1) Smith, P. J.; Wang, H.-T.; York, W. S.; Peña, M. J.; Urbanowicz, B. R. Designer biomass for next-generation biorefineries: leveraging recent insights into xylan structure and biosynthesis. *Biotechnol. Biofuels* **2017**, *10*, No. 286.

(2) Scheller, H. V.; Ulvskov, P. Hemicelluloses. *Annu. Rev. Plant Biol.* **2010**, *61*, 263−289.

(3) Kang, X.; Kirui, A.; Widanage, M. C. D.; Mentink-Vigier, F.; Cosgrove, D. J.; Wang, T. Lignin-polysaccharide interactions in plant secondary cell walls revealed by solid-state NMR. *Nat. Commun.* **2019**, *10*, No. 347.

(4) Simmons, T. J.; Mortimer, J. C.; Bernardinelli, O. D.; Pöppler, A.-C.; Brown, S. P.; Deazevedo, E. R.; Dupree, R.; Dupree, P. Folding of xylan onto cellulose fibrils in plant cell walls revealed by solid-state NMR. *Nat. Commun.* **2016**, *7*, No. 13902.

(5) Peng, X.; Du, F.; Zhong, L. Synthesis, Characterization, and Applications of Hemicelluloses Based Eco-Friendly Polymer Composites. *Sustainable Polymer Composites and Nanocomposites*; Springer, 2019; pp 1267−1322.

(6) Grondin, J. M.; Tamura, K.; Déjean, G.; Abbott, D. W.; Brumer, H. Polysaccharide utilization loci: fueling microbial communities. *J. Bacteriol.* **2017**, *199*, No. e00860-16.

(7) Cartaxo da Costa Urtiga, S.; Marcelino, H. R.; do Egito, E. S. T.; Oliveira, E. E. Xylan in drug delivery: A review of its engineered structures and biomedical applications. *Eur. J. Pharm. Biopharm.* **2020**, *151*, 199−208.

(8) Smith, P. J.; Ortiz-Soto, M. E.; Roth, C.; Barnes, W. J.; Seibel, J.; Urbanowicz, B. R.; Pfrengle, F. Enzymatic synthesis of artificial polysaccharides. *ACS Sustainable Chem. Eng.* **2020**, *8*, 11853−11871.

(9) Moremen, K. W.; Haltiwanger, R. S. Emerging structural insights into glycosyltransferase-mediated synthesis of glycans. *Nat. Chem. Biol.* **2019**, *15*, 853−864.

(10) Lairson, L.; Henrissat, B.; Davies, G.; Withers, S. Glycosyltransferases: structures, functions, and mechanisms. *Annu. Rev. Biochem.* **2008**, *77*, 521−555.

(11) Urbanowicz, B. R.; Peña, M. J.; Moniz, H. A.; Moremen, K. W.; York, W. S. Two Arabidopsis proteins synthesize acetylated xylan in vitro. *Plant J.* **2014**, *80*, 197−206.

(12) Jensen, J. K.; Busse-Wicher, M.; Poulsen, C. P.; Fangel, J. U.; Smith, P. J.; Yang, J. Y.; Pena, M. J.; Dinesen, M. H.; Martens, H. J.; Melkonian, M.; Wong, G. K.; Moremen, K. W.; Wilkerson, C. G.; Scheller, H. V.; Dupree, P.; Ulvskov, P.; Urbanowicz, B. R.; Harholt, J. Identification of an algal xylan synthase indicates that there is functional orthology between algal and plant cell wall biosynthesis. *New Phytol.* **2018**, *218*, 1049−1060.

(13) Kobayashi, S.; Wen, X.; Shoda, S.-i. Specific preparation of artificial xylan: a new approach to polysaccharide synthesis by using cellulase as catalyst. *Macromolecules* **1996**, *29*, 2698−2700.

(14) Senf, D.; Ruprecht, C.; Kishani, S.; Matic, A.; Toriz, G.; Gatenholm, P.; Wågberg, L.; Pfrengle, F. Tailormade polysaccharides with defined branching patterns: enzymatic polymerization of arabinoxylan oligosaccharides. *Angew. Chem., Int. Ed.* **2018**, *57*, 11987−11992.

(15) Yundt, A. P. The Preparation, Characterization, and Hydrolysis of Crystalline and Amorphous Xylan. Ph.D. Thesis, Georgia School of Technology, Lawerence College: Appletin, WI, 1949. https://smartech.gatech.edu/handle/1853/7076.

(16) Chanzy, H.; Comtat, J.; Dube, M.; Marchessault, R. Enzymatic degradation of β (1→ 4) xylan single crystals. *Biopolymers* **1979**, *18*, 2459−2464.

(17) Chanzy, H.; Dube, M.; Marchessault, R. Structural polymorphism of (1→ 4)—β—d—Xylan. *Polymer* **1979**, *20*, 1037−1039.

(18) Marchessault, R.; Morehead, F.; Walter, N.; Glaudemans, C.; Timell, T. Morphology of xylan single crystals. *J. Polym. Sci.* **1961**, *51*, S66−S68.

(19) Bishop, C. Crystalline xylans from straws. *Can. J. Chem.* **1953**, *31*, 793−800.

(20) Meng, Z.; Sawada, D.; Laine, C.; Ogawa, Y.; Virtanen, T.; Nishiyama, Y.; Tammelin, T.; Kontturi, E. Bottom-up Construction of Xylan Nanocrystals in Dimethyl Sulfoxide. *Biomacromolecules* **2021**, *22*, 898−906.

(21) Bosmans, T. J.; Stépán, A. M.; Toriz, G.; Renneckar, S.; Karabulut, E.; Wågberg, L.; Gatenholm, P. , Assembly of debranched xylan from solution and on nanocellulosic surfaces. *Biomacromolecules* **2014**, *15*, 924−930.

(22) Wang, S.; Xiang, Z. Highly Stable Pickering Emulsions with Xylan Hydrate Nanocrystals. *Nanomaterials* **2021**, *11*, No. 2558.

(23) Simmons, T. J.; Mortimer, J. C.; Bernardinelli, O. D.; Poppler, A. C.; Brown, S. P.; Deazevedo, E. R.; Dupree, R.; Dupree, P. Folding of xylan onto cellulose fibrils in plant cell walls revealed by solid-state NMR. *Nat. Commun.* **2016**, *7*, No. 13902.

(24) Chang, Y. L.; Liao, S. K. S.; Chen, Y. C.; Hung, W. T.; Yu, H. M.; Yang, W. B.; Fang, J. M.; Chen, C. H.; Lee, Y. C. Tagging saccharides for signal enhancement in mass spectrometric analysis. *J. Mass Spectrom.* **2011**, *46*, 247−255.

(25) Busse-Wicher, M.; Gomes, T. C.; Tryfona, T.; Nikolovski, N.; Stott, K.; Grantham, N. J.; Bolam, D. N.; Skaf, M. S.; Dupree, P. The pattern of xylan acetylation suggests xylan may interact with cellulose microfibrils as a twofold helical screw in the secondary plant cell wall of Arabidopsis thaliana. *Plant J.: Cell Mol. Biol.* **2014**, *79*, 492−506.

(26) Wang, H.-T.; Bharadwaj, V. S.; Yang, J. Y.; Curry, T. M.; Moremen, K. W.; Bomble, Y. J.; Urbanowicz, B. R. Rational enzyme design for controlled functionalization of acetylated xylan for cell-free polymer biosynthesis. *Carbohydr. Polym.* **2021**, *273*, No. 118564.

(27) Faijes, M.; Imai, T.; Bulone, V.; Planas, A. In vitro synthesis of a crystalline (1 3, 1 4)-beta-d-glucan by a mutated (1 3, 1 4)-beta-d-glucanase from Bacillus. *Biochem. J.* **2004**, *380*, 635−641.

(28) Gullfot, F.; Ibatullin, F. M.; Sundqvist, G.; Davies, G. J.; Brumer, H. Functional characterization of xyloglucan glycosynthases from GH7, GH12, and GH16 scaffolds. *Biomacromolecules* **2009**, *10*, 1782−1788.

(29) Tsai, T.-I.; Lee, H.-Y.; Chang, S.-H.; Wang, C.-H.; Tu, Y.-C.; Lin, Y.-C.; Hwang, D.-R.; Wu, C.-Y.; Wong, C.-H. Effective sugar nucleotide regeneration for the large-scale enzymatic synthesis of Globo H and SSEA4. *J. Am. Chem. Soc.* **2013**, *135*, 14831−14839.

(30) Anwar, M. T.; Kawade, S. K.; Huo, Y.-R.; Adak, A. K.; Sridharan, D.; Kuo, Y.-T.; Fan, C.-Y.; Wu, H.-R.; Lee, Y.-S.; Angata, T.; Lin, C.-C. Sugar nucleotide regeneration system for the synthesis of Bi-and triantennary N-glycans and exploring their activities against siglecs. *Eur. J. Med. Chem.* **2022**, *232*, No. 114146.

(31) Moremen, K. W.; Ramiah, A.; Stuart, M.; Steel, J.; Meng, L.; Forouhar, F.; Moniz, H. A.; Gahlay, G.; Gao, Z.; Chapla, D.; et al. Expression system for structural and functional studies of human glycosylation enzymes. *Nat. Chem. Biol.* **2018**, *14*, 156.

(32) Eames, B. F.; Singer, A.; Smith, G. A.; Wood, Z. A.; Yan, Y.-L.; He, X.; Polizzi, S. J.; Catchen, J. M.; Rodriguez-Mari, A.; Linbo, T.; et al. UDP xylose synthase 1 is required for morphogenesis and histogenesis of the craniofacial skeleton. *Dev. Biol.* **2010**, *341*, 400−415.

(33) Schneider, C. A.; Rasband, W. S.; Eliceiri, K. W. NIH Image to ImageJ: 25 years of image analysis. *Nat. Methods* **2012**, *9*, 671−675.

https://doi.org/10.1021/acsmaterialsau.2c00006
ACS Mater. Au 2022, 2, 440−452